Advances in Materials Research, *Vol. 15, No. 1 (2026) 49-68*
https://doi.org/10.12989/amr.2026.15.1.049

Techno-Press

Development of GGBS based high-strength one-part geopolymer concrete and its properties

Divya Sharma, Ran Bir Singh*

Department of Civil Engineering, Central University of Haryana, Mahendergarh, 123031, India

(Receive August 19, 2025, Revised January 26, 2026, Accepted January 27, 2026)

Abstract. The study presents a rational approach for design and optimization of high-strength One-Part Geopolymer Concrete (OP-GPC) mixes for a targeted compressive strength of 70 MPa using Response Surface Methodology (RSM). The model generated through RSM showed significant statistical relationship between the selected input and output variables. The high-strength OP-GPC was designed with ground granulated blast furnace slag as primary binder and anhydrous sodium metasilicate as the solid activator. The RSM model established statistically significant relationships between design parameters and compressive strength, which were subsequently validated through laboratory experimentation. The optimized OP-GPC have achieved compressive strength in the range of 70 MPa-76 MPa at 28 day. The experiments showed that approximately 90% of the targeted compressive strength was achieved within initial 7 days. The mechanical performance of high-strength OP-GPC was measured in terms of flexural and split-tensile strengths which was measured at 7.37 MPa and 5.32 MPa at 28 days, respectively. The durability of high-strength one-part GPC was also measured which showed low permeable void content of 8.17%, sorptivity of 0.0010 mm/s$^{1/2}$ and chloride penetration depth of 5.81 mm at 180 days that indicated superior performance relative to conventional concrete. The results demonstrated that the proposed RSM-based design approach enables the development of high-strength OP-GPC with superior mechanical and durability performance. The optimized high-strength OP-GPC is recommended for sustainable and high-performance structural applications, particularly where early-age strength development and enhanced durability under aggressive exposure conditions is also needed.

Keywords: durability properties; ground granulated blast furnace slag; high-strength concrete; mechanical properties; one-part geopolymer concrete; response surface methodology

1. Introduction

As per BIS 456 [1], the high-strength concrete exhibits the compressive strength greater than 55 MPa. Neupane [2], have reported that high-strength concrete replaced the large volume concrete to slim sections that ultimately reduced dead load, cost and time. It was also noted that high-strength concrete has wide application in skyscraper developments, bridge engineering and pre-stressed structural elements. The high-strength concrete was also made with geopolymer technology that further reduced dependency on cement and carbon emissions by up to 70% [3]. Weil et al. [4] have reported that GPC can reduce the greenhouse gas emissions by approximately 75% compared to traditional concrete. The design of high-strength conventional GPC has been

*Corresponding author, Ph.D., Assistant Professor, E-mail: ranbirsingh@cuh.ac.in

Copyright © 2026 Techno-Press

ISSN: 2234-0912 (Print), 2234-179X (Online)

addressed in previous research [5-9]. The drawbacks of GPC including heat curing and two-step preparation of activating solution was resolved by the advanced technology termed as one-part geopolymer concrete [10-15].

The major constituent of one-part geopolymer concrete is alumino-silicate-precursor (single or in combination) for example Ground Granulated Blast Furnace Slag (GGBS), metakaolin, fly ash and rice husk ash. The precursors are activated by solid alkali activators [16-19]. A few studies have investigated the high-strength based one-part geopolymer research to mortar-level. According to Dong et al. [20] have reported that one-part geopolymer mortars was prepared with solid sodium metasilicate of constant silicate modulus of 0.97. The binder was having different fly ash to GGBS ratios of i.e. 80 to 20, 40 to 60 and 0 to 100. The water-to-binder ratio was ranged from 0.31 to 0.37. The high-strength one-part geopolymer mortars prepared with solid activators demonstrated superior compressive strength of 80 to 105 MPa compared to mixes prepared with liquid activators. Dakhane and Neithalath [21] have reported the effect of powdered silicates on strength development of GGBS-based high-strength one-part alkali-activated binders. It was noted that silicate-activated mortars can achieve compressive strengths exceeding 80 MPa at 56 days and upto 30 MPa in 72 hrs. depending on design parameters. The design parameters affected the behaviour was total alkalinity, silica modulus and type of activator cation.

In literature, very few studies have addressed the mix. design strategies of high-strength OP-GPC. Manjunath et al. [22] noted the bond strength properties of high-strength OP- GPC and reported the compressive strength ranging from 76 to 91 MPa and bond strength between 12 to 14 MPa. The authors have noted the bond-strength is directly proportional to compressive strength. Araújo-Júnior et al. [23] have reported hardened properties of high-strength slag-based concrete. The compressive strength of the concrete increased rapidly, reaching values above 41 MPa at 1 day. At 28 days, the compressive strength ranged between 86 MPa and 105 MPa depending on the mix proportions. The rapid strength gain was attributed to the low water-to-binder (w/b) ratios (0.28, 0.36, and 0.44) and the use of sodium silicate activators with a silica modulus of 1.78 and Na_2O content of 4.5%. Using the RSM model, Sharma and Singh [24] identified optimal mix proportions and further validated the model in the laboratory and achieved compressive strengths up to 55 MPa. Kurtoglu et al. [25] have reported the application of advanced machine learning techniques to predict the residual compressive strength of GGBS and Fly ash based geopolymer concretes. The authors have identified temperature, water content, aggregate proportions, silicate/hydroxide ratio and curing conditions as the most influential variables with 95% of model predictive accuracy. Paruthi et al. [26] have compared different machine learning algorithms for predicting the compressive strength of GGBS-based geopolymers and found Gradient Boosting Machine to be the most reliable for the low prediction error and high correlation. Their findings support the integration of data-driven techniques and experimental validation of mix design. Al-Rousan and Sawalha [27] have investigated the structural behavior of square concrete-filled steel tubular columns incorporating high-strength geopolymer concrete as the infill. The results showed that the factors such as binder chemistry, gel phases and steel tube thickness significantly influenced the load-bearing capacity, stiffness, energy absorption and ductility of the column. From the literature it is evident that investigations on high-strength one-part geopolymer concrete remains limited, particularly for performance prediction of mix design using machine learning approaches.

Khater and Abd el Gawaad [28] reported that the addition of 0.1% carbon nanotube in slag-based geopolymer mortar reduced water absorption and shrinkage whereas high dosage led to agglomeration and deterioration of durability properties. The recent investigations on GGBS–

metakaolin blends have reported compressive strengths of 36 MPa with excellent durability including better resistance to acid attack and high temperatures compared to conventional concrete [29]. Zedan et al. [30] demonstrated that incorporating GGBFS into alkali-activated ceramic waste systems significantly enhanced compressive strength and microstructural compaction whereas substitution with concrete waste reduced performance. The existing durability investigations provide valuable insights however there remains a clear gap in understanding the durability of high-strength one-part GPC.

The optimisation of design parameters and also durability analysis of high-strength OP-GPC remains underexplored. To fill this research gap, the primary objective of the present study is to optimize the mix design of high-strength OP- GPC through RSM and further analyse its mechanical and durability properties. The study specifically targeted a high compressive strength of 70 MPa at 28 days for the design of high-strength OP- GPC. The study has analysed model's prediction and validated the predicted compressive strength in laboratory. The fresh, mechanical and durability behaviour of high-strength OP- GPC was analysed.

2. Research significance

In the technical literature, researchers have designed and studied high-strength two-part GPC for a targeted compressive strength up to 85 MPa. However, a few studies focused on high-strength one-part GPC designed in the strength range of 60-90 MPa using precursors like GGBS, rice husk ash, fly ash and activators like sodium silicate. There exists a gap in technical literature regarding design mix approach and methodology for high-strength OP-GPC. The present study addressed the gaps and highlighted a rational mix design approach for design mix of GGBS based high-strength OP-GPC through RSM. The model was further validated with laboratory experiments. The study also explored experimentally the mechanical and durability behaviour of the designed high-strength OP-GPC through RSM.

3. Methodology

3.1 Modeling

The Response Surface Methodology (RSM) was used to design high-strength OP-GPC to attain the strength of 70 MPa. RSM is a statistical tool used to develop models that describe the relationship between input parameters and output variables [31]. The model analysed the data set and facilitated evaluation of the influence of factors, their interactions and process optimization. The application of RSM for optimization of mix design involves several stages, including factor selection, experimental design, appropriate model selection, model adequacy verification, graphical representation and final optimization [32]. The data for mix. design of high-strength OP-GPC made with GGBS and anhydrous sodium metasilicate were compiled from previously published research [33-40]. A dataset of 100 points was analysed, considering independent variables like GGBS, coarse aggregate, water, fine aggregate and anhydrous sodium metasilicate (measured in kg/m^3). The compressive strength (MPa) was selected as the dependent variable. The minimum and maximum range of parameters were defined as per the technical literature. The nomenclature and ranges of the factors used in the model for designing high-strength OP- GPC were analysed through RSM.

The materials used for designing high-strength OP-GPC on RSM were GGBS used in amounts from 0 to 600 kg per cubic meter, with an average of about 239.5 kg/m³. The activator anhydrous sodium metasilicate ranged from 0 to about 162 kg /m³, with an average of about 81.4 kg/m³. The content of water ranged between 57 and 249 kg/m³, averaging 130.9 kg/m³. The coarse aggregates were used from 825 to 1242.5 kg/m³ averaging 1084.9 kg/m³. The fine aggregates ranged from 457.5 to 805 kg/m³ and the average amount was 691.3 kg/m³. The above mentioned values were determined through RSM based on the data collected from the literature. The proposed approach offered a well-organized framework for optimizing and validating the study's output parameters. The process was carried out step by step, beginning with identifying the problem and selecting parameters based on literature. The selected input factors and output parameter were then utilized for model optimization and implementing statistical method to address the complex relationships among these variables. The optimal design method in RSM was applied and the Two-Factor Interaction (2-FI) statistical technique was identified as the most suitable for the given data set. Statistical analysis was conducted to refine the p-value, R^2 value and F-value that improved the accuracy of RSM model. The 2D-contour plots were further generated to demonstrate the influence of input parameters on output value. The final mix design was obtained from the optimized contour plots and subsequently validated through laboratory experiments. The model was validated by adopting the optimized conditions in the laboratory and comparing the predicted results with the experimental findings.

3.2 Materials

High-strength OP-GPC mix designs generated by RSM was experimentally authenticated in the host institution’s laboratory. For development of high-strength OP-GPC, GGBS was used in the form of alumino-silicate precursor and granular anhydrous sodium metasilicate was used as an activator. The GGBS used in this study met the specifications outlined in BIS 16714 [41] and exhibits specific gravity of 2.89 and Blaine fineness of 382 m²/kg. The GGBS met the Indian standard requirements, with a $(CaO + MgO + Al_2O_3)/SiO_2$ ratio of 1.8 and a glass content of 96.60%. The activator comprised of 49.82% SiO_2 and 50.50% Na_2O, with a measured silica modulus ratio of 0.98. As specified by BIS 383 [42], the aggregates incorporated in the research work included coarse aggregates up to 20 mm and fine aggregates under 4.75 mm. The specific gravity measured was 2.60 for the fine aggregates and 2.80 for the coarse aggregates. The aggregates exhibited an impact value of 15.35% and a Los Angeles abrasion value of 26.16, both falling within the limits specified by BIS 2386 [43]. In the laboratory, high-strength OP-GPC was prepared using a pan mixer. Initially, the GGBS and anhydrous sodium metasilicate were blended together in dry state. Further, the coarse and fine aggregates were added and dry mixing was carried for one minute to achieve a uniform blend. The water was then added in three stages: the first one-third portion of total water was poured and mixed for one minute, followed by the next one-third portion mixed for another one minute. In the end, the residual portion of water was incorporated and mixed for the final one minute.

3.3 Testing

The consistency, IST and FST were measured for high-strength OP-GPC following BIS 4031 [44]. The high-strength OP-GPC was tested for workability with the standard slump cone in accordance to BIS 1199 [45].

The compressive strength of high-strength OP-GPC was tested on cubic samples of standard

size 150×150×150 mm. The compressive strength of high-strength OP- GPC were determined at 7 and 28 days of water curing in accordance to BIS 516 [46]. The flexural strength of the high-strength OP-GPC was measured on beam specimens of standard size 100×100×500 mm in accordance to BIS 516 [46]. The cylindrical specimens of standard size 100×200 mm was used to determine split-tensile strength following the guidelines of BIS 5816 [47]. The flexural and split-tensile strength of high-strength OP- GPC were evaluated at a duration of 28 and 90 days of water curing.

The cylindrical samples of standard size- 100×200 mm was used to determine sulphate resistance, chloride resistance, density, water absorption, void content and sorptivity. The durability of high-strength OP-GPC against sulphate attack was tested by submerging samples in a 5% solution of magnesium sulphate. The resistance to sulphate exposure was evaluated at 28, 56, 90, 120 and 180 days of immersion. The assessment criteria included was visual inspection, weight loss and compressive strength degradation in accordance to GB/T 50082 [49].

The chloride resistance of high-strength OP-GPC was evaluated based on chloride penetration depth. The chloride penetration depths were determined with water-cured cylindrical specimens that were immersed in a 5% sodium chloride solution for 56, 90, 120, and 180 days of exposure in accordance to ASTM C1556 [50]. To determine penetration depth, the cylindrical samples were split and further 0.1N $AgNO_3$ (silver nitrate) solution was sprayed on the exposed surfaces. Additionally, the loss in weight of the samples were recorded and further analysed.

The high-strength OP-GPC were assessed for density, water absorption and void content following ASTM C642 [51]. The bulk density, apparent bulk density and the percentage of permeable voids were also determined for the high-strength OP-GPC.

The sorptivity of high-strength OP-GPC was evaluated using the capillary suction test following ASTM C1585 [52]. The test was conducted on disc specimens measuring 100×200 mm after 90 days of water curing. Water cured samples were placed in an oven for 72 hours to dry and further cooled before testing. To ensure controlled absorption, all sides of the discs were wrapped with wax while only the top surface remained unprotected. The prepared specimens were placed in water with base support, maintaining a water-level of 1-3 mm on exposed surface. Weight of specimens was recorded at intervals ranging from one minute to six hours to determine primary absorption, while secondary absorption was assessed over a period of one to seven days. Correlations between initial absorption (mm) and time ($sec^{1/2}$), as well as secondary absorption (mm) and time ($sec^{1/2}$), were established and analysed for high-strength OP- GPC.

The water penetration depth of high-strength OP-GPC was evaluated with cube specimens of standard size 150×150×150 mm following BIS 516 Part 2: Sec 1 [53]. Following the test, the samples were split in two parts to measure the extent of water penetration depth. The initial surface absorption test for high-strength OP- GPC was carried out following BS 1881: Part 208 [54] and BS EN 12390-2 [55] to determine the rate of initial surface absorption. The sample preparation was conducted as per standard procedures to ensure a consistent mass before testing.

4. Results and discussions

4.1 Statistical analysis of the model

The dataset was analysed with four statistical models namely Quadratic, Cubic, 2-FI and Linear. Analysis of the model includes desired value of the R^2, the p-value, the predicted R^2 and the

Table 1. ANOVA results for high-strength OP-GPC

Source	Sum of Squares	df	Mean Square	F-value	p-value	Remarks
Model	12900.82	12	1075.07	15.21	< 0.0001	significant
A-GGBS	863.71	1	863.71	12.22	0.0020	-
C-ASM*	4496.15	1	4496.15	63.62	< 0.0001	-
D-Water	285.21	1	285.21	4.04	0.0570	-
E-Coarse Aggregates	68.05	1	68.05	0.9629	0.3371	-
F-Fine Aggregates	193.57	1	193.57	2.74	0.1121	-
AC	424.45	1	424.45	6.01	0.0227	-
BF	557.44	1	557.44	7.89	0.0102	-
CD	1834.28	1	1834.28	25.96	< 0.0001	-
CF	1825.46	1	1825.46	25.83	< 0.0001	-
DE	1075.41	1	1075.41	15.22	0.0008	-
DF	1092.96	1	1092.96	15.47	0.0007	-
Residual	1554.74	22	70.67	-	-	-
Lack of Fit	1311.58	19	69.03	0.8517	0.6542	not significant
Pure Error	243.16	3	81.05	-	-	-
Cor Total	14455.57	34	-	-	-	-

*ASM-Anhydrous sodium metasilicate

adjusted R^2 that indicates the predictive accuracy of model. The initial summary of different statistical models was produced the linear model had a sequential p-value of 0.0129 and a lack of fit p-value of 0.1381, with R^2, adjusted R^2 and predicted R^2 values of 0.4182, 0.2935, and 0.5299, respectively and reported a poor fit. The 2FI model showed the best results, with sequential p-value below 0.0002, lack of fit p-value of 0.7106 and R^2, adjusted R^2 and predicted R^2 values of 0.9442, 0.8540 and 0.7512. The quadratic model had a high sequential p-value of 0.1834 and a lack of fit p-value of 0.9508 with R^2 and adjusted R^2 values of 0.9798 and 0.9019, hence not recommended. The cubic model, although it had the highest R^2 value of 0.9832, but was aliased and therefore not considered reliable. Based on these results, the 2FI model was suggested for further analysis, as it offered the best overall fit to the data.

The significant factors were determined by applying the Analysis of Variance (ANOVA) technique. The model was validated with the F-and p-value of the 2FI-model. RSM optimized the input factors to obtain the targeted output. Table 1 presents the ANOVA results for M70 grade OP-GPC. The results indicated the significant model with the F-value of 15.21 implies the model is significant. The p-value of less than 0.0001 also indicated that model terms are significant. In the present study A, C, AC, CD, CF, DE and DF are significant model terms with p-values of 0.0020, <0.0001, 0.0227, <0.0001, 0.0008 and 0.0007, respectively, which indicated that aforesaid terms were significant model terms. Among the individual factors C demonstrates the most substantial effect with the highest F-value (63.62) and a p-value of less than 0.0001 highlighting its critical role in influencing the response. Similar, interactions between variables such as AC, CD, CF, DE, and DF were shown to contribute significantly to the model, with their p-values being less than 0.05, underscoring the importance of combined factor effects. The Lack of Fit p-value and Lack of Fit F-value of 0.8517 and 0.6542, respectively in the table implies that Lack of

Table 2. Statistical summary of the RSM model

Source	SD	Adj.-R^2	Mean	C.V. %	Pred.- R^2	R^2	AP	Remark
2FI-Model	8.41	0.8338	62.43	13.47	0.7512	0.8924	14.63	M70 grade

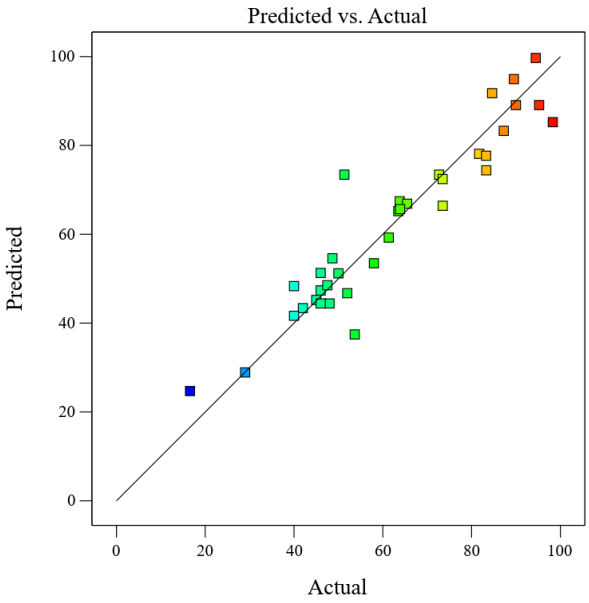

Figure 1. Correlation between actual and predicted compressive strength for high-strength OP- GPC

Fit is not significant relative to pure error. The non-significant lack of fit was acceptable for the model fitness. Numerous researchers have used RSM to optimize geopolymer concrete [56-58]. In the present study, the model exhibited a strong fit with an R^2 value of 0.8924, supported by a significant p-value (<0.0001). The results demonstrated the optimization of mix of materials and their interactions to achieve the best possible results. The performance of the statistical model was determined in terms of model R^2 value, Standard Deviation (SD) and Coefficient of Variation in percentage (CV%). The predicted R^2 value of 0.7512 was reasonably in good agreement with the adjusted R^2 value of 0.8338 with a difference of less than 0.2. The adequate precision value defines the signal-to-noise ratio and a value of more than 4 is considered to be favourable [59]. The model provides an Adequate Precision (AP) value of 14.63 which indicates a strong signal and holds significance, Table 2.

The model statistics clearly indicated that the model is suitable for navigating the design space effectively. The statistical performance of the model demonstrated a notable correlation between the input and the output variables which was further confirmed by ANOVA analysis. As illustrated in Fig. 1, there is minimal variation between the model's predicted compressive strength and the actual measured values.

4.2 Contour plots

To achieve the target compressive strength of 70 MPa, the 2D-contour plots were generated through RSM to explore the effects of factors and their combinations on output parameter. The

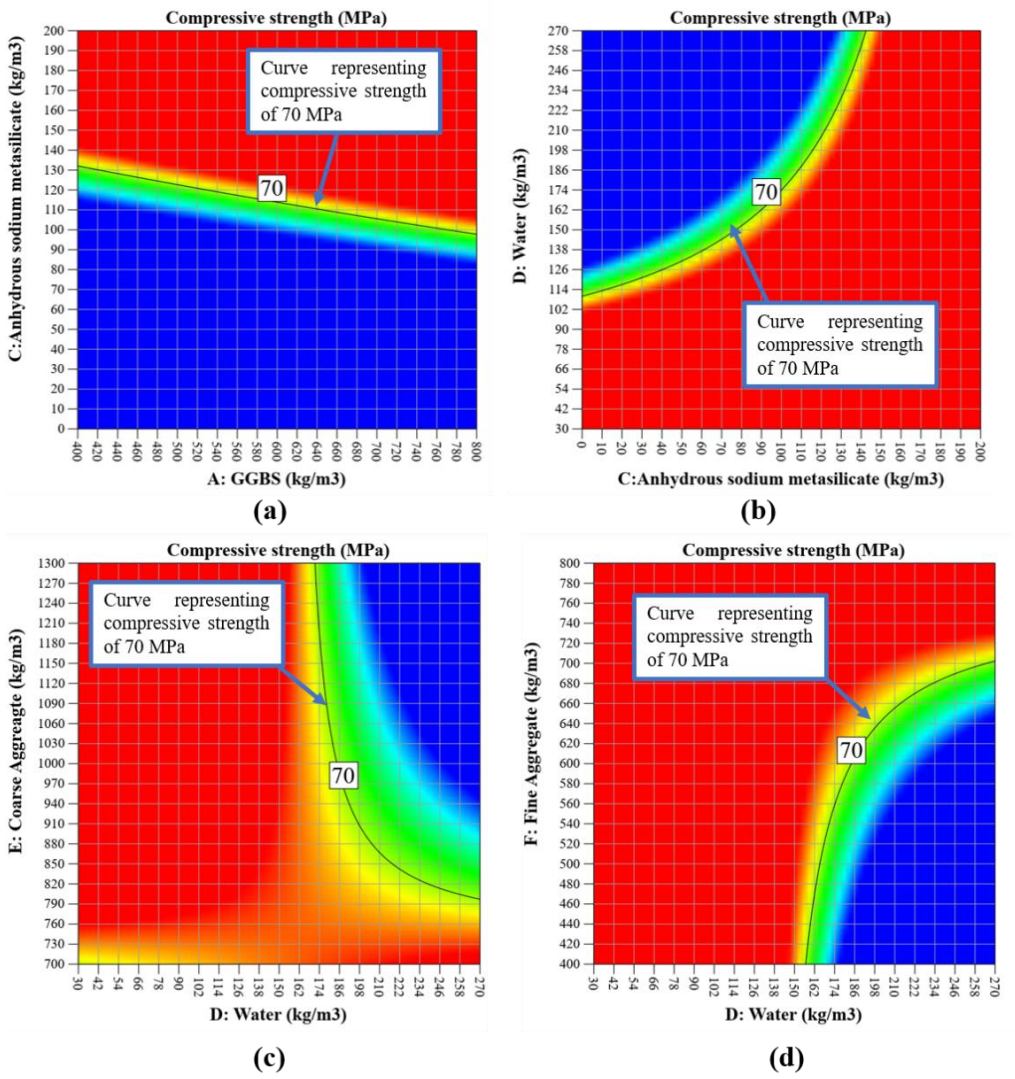

Figure 2. 2-D contour plots generated from RSM for high-strength OP-GPC

Fig. 2 demonstrates 2D-contour plots, that exhibits the interaction of input factors to and corresponding output value. The research aimed to optimize the mix proportion of high-strength OP-GPC made with a single precursor and activator. The objective was to optimize the activator content to reach high compressive strength. The plots supported to identify best possible values of different parameters and exhibited the output parameter value.

Fig. 2(a) presents the interaction between parameters A (GGBS content) and C (anhydrous sodium metasilicate content). The contour plots provide the amount of GGBS content from 400-800 kg/m³ on the x-axis and the amount of anhydrous sodium metasilicate content from 0-200 kg/m^3 on the y-axis. Fig. 2(b) presents a 2D-contour plot presents the interaction of parameters C and D (water content). The x-axis represents factor ‘C’ while the y-axis shows factor ‘D’ with content of 30–270 kg/m³ based on the input data range. Fig. 2(c) illustrates the interaction between

Table 3. High-strength OP-GPC mix compositions optimized using RSM

Mix. constituents	Mix designation				
	HSC-1	HSC-2	HSC-3	HSC-4	HSC-5
GGBS (kg/m^3)	560	580	600	620	640
Anhydrous sodium metasilicate (kg/m^3)	119	117	115	112	110
Water (kg/m^3)	202	200	198	196	186
Coarse aggregates (kg/m^3)	890	900	910	920	950
Fine aggregates (kg/m^3)	650	640	630	620	610
Binder Content (kg/m^3)	679	697	715	732	750
W/B ratio	0.30	0.29	0.28	0.27	0.25

factors D and E (coarse aggregate content) produced in RSM. The plots provide the amount of water content (kg/m^3) on the x-axis and y-axis shows factor 'E' ranging from 700–1300 kg/m^3 based on the input data range. Fig. 2(d) illustrates the relationship between parameters D (water content) and F (fine aggregate content) generated in RSM in terms of 2D contour plots for the high-strength OP- GPC. The plots illustrate the amount of water content (kg/m^3) on the x-axis and the amount of fine aggregate (kg /m^3) on the y-axis. Fig. 2(d) shows the range of factor 'F' from 400-800 kg/m^3 suggested by RSM based on the dataset. The plots were used to extract mix. proportions for high-strength OP- GPC.

4.3 Experimental validation

The high-strength OP-GPC were designed through the RSM model and validated through laboratory experiments. The mix. proportions were determined using the contour plots by following the procedure discussed in section 4.2. The five distinct mix designs were obtained from the model. For each mix, three concrete cubes were cast, resulting in a total of fifteen specimens for validation purposes. The detailed compositions for each of the five M70 grade mixes derived from RSM are summarized in Table 3, labelled as HSC-1 to HSC-5. The binder content of the mix ranged from 679 to 750 kg/m^3. Across the five mixes, the w/b ratio varied between 0.30 and 0.25. The proportion of activator in HSC-1, HSC-2, HSC-3, HSC-4 and HSC-5 was 17.53%, 16.78%, 16.08%, 15.30%, and 14.67%, respectively. Further, it may also be noted that the dosage of anhydrous sodium metasilicate decreases with an increase in the binder content, as shown in Table 3. This indicates a trend of reducing activator dosage as the GGBS content increases, while maintaining the targeted compressive strength. For example, the requirement of anhydrous sodium metasilicate content was 17.47 % for mix HSC-1 at a binder content of 679 kg/m^3 which was decreased to 14.67% in mix HSC-5 at a binder content of 750 kg/m^3.

For model validation, concrete cubes corresponding to each mix in Table 3 were casted in the laboratory. Analysis of the results demonstrated that mix. HSC-5 had low w/b ratio compared to HSC-1, as presented in Table 3. The reduced w/b ratio resulted in low slump value of 60 mm for mix HSC-1 at a w/b ratio of 0.30 and 25 mm for mix HSC-5 at a w/b ratio of 0.25, Table 4.

The 28-day compressive strength of water-cured concrete cubes are also presented in Table 4. The aforesaid table revealed that mixes HSC-1, HSC-2, HSC-3, HSC-4 and HSC-5 attained compressive strengths of 71.34 MPa, 72.12 MPa, 73.50 MPa, 73.87 MPa, and 74.02 MPa, respectively. It is noteworthy that the measured compressive strengths exceeded the target value of

Table 4. Experimental results of slump and compressive strength for high-strength OP-GPC

Concrete Grade	Mix ID	Slump (mm)	Target CS* (MPa)	Measured CS (MPa)	Difference (%)
High-strength	HSC-1	60	70	71.34	1.91
	HSC-2	55	70	72.12	3.32
	HSC-3	50	70	73.50	5.00
	HSC-4	42	70	73.87	5.52
	HSC-5	25	70	74.02	5.74

*CS- Compressive strength

70 MPa. This suggests that the developed model underestimated the optimal mix design for high-strength OP-GPC. The percentage deviations calculated between predicted and measured values are reported in Table 4 which revealed a variation in the range of 1% to 5% for high-strength OP-GPC. Notably, the measured compressive strength values were consistently high than the predicted values which confirmed the conservative nature of the developed model. The model developed in the present study provides a practical resource for practitioners to finalize the mix proportions of high-strength concrete according to the demands of different applications. From the extracted design mixes, Table 3, HSC-3 design mix was selected for testing the fresh and hardened state properties of high-strength OP- GPC.

4.4 Fresh and Hardened state properties

The consistency, IST and FST measured for high-strength OP-GPC was 28%, 38 minutes and 120 minutes, respectively. The measured values of consistency, IST and FST of OP- GPC made with GGBS and anhydrous sodium metasilicate with same dosage of activator are in line with the available literature. Slump value obtained for high-strength OP-GPC was 50 mm which confirms to ‘medium workability class’ as per the requirements of BIS:456 [1]. The low workability class of high-strength OP-GPC is attributed to the significant powder content (precursor + activator) and low w/b ratio of 0.28.

The measured value of compressive strength of high- strength OP- GPC at 7 and 28 days were 66.14 MPa and 71.25 MPa, respectively. The targeted high-compressive strength at 28 days was achieved following BIS 456 [1]. The analysis of obtained results exhibited that more than 90% of the strength was achieved at 7 days for high-strength OP- GPC. Teo et al. [60] have reported that OP-GPC designed with GGBS and anhydrous sodium metasilicate have achieved 85% of the total compressive strength within the one week. Unlike OP-GPC, conventional cement concrete generally develops only 65–70% of its final strength within the first week [61-64]. The faster strength gain seen in OP-GPC is mainly due to high reactivity of the binders and the rapid formation of geopolymer gel, also reported in previous research [65-68]. The rapid early-age strength development observed in the high-strength OP-GPC system is primarily attributed to the high alkalinity of the powdered activator and the optimized silica modulus that accelerated the dissolution of reactive aluminosilicate and calcium-bearing phases in the precursor. This process promoted the early formation of a dense and well-polymerized C-(A)-S-H/N-A-S-H hybrid gel network and resulted in rapid matrix densification and refinement of the pore structure. The calcium-rich nature of the binder further facilitated the precipitation of C-(A)-S-H-type reaction products, which contributed significantly to early stiffness and strength.

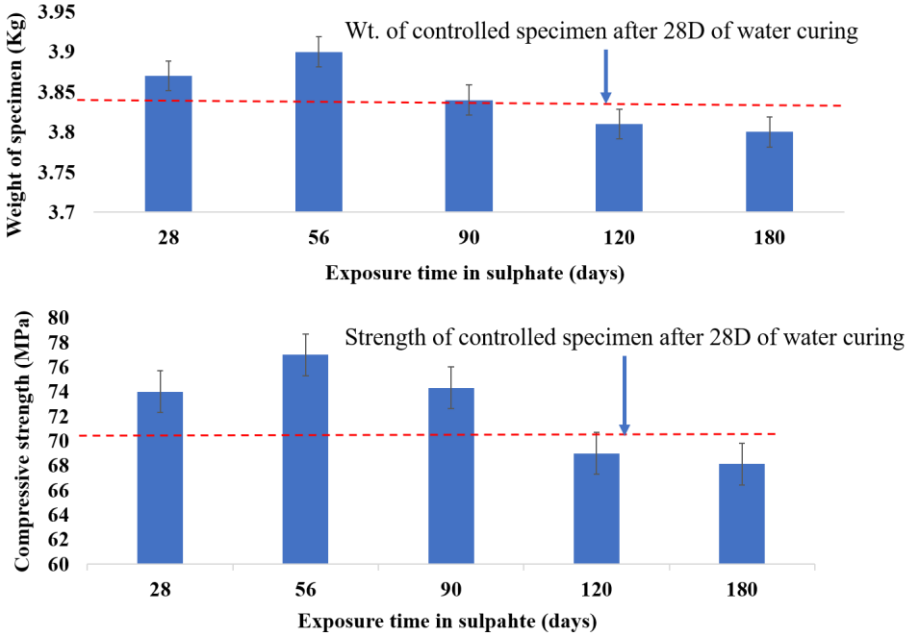

Figure 3. Sulphate resistance of high-strength OP- GPC measured in terms of (a) weight loss and (b) the strength loss

For high-strength OP-GPC, flexural strength of mixes reported was reported 7.37 MPa after 28 days that enhanced to 8.08 MPa after a duration of 90 days. Split-tensile strength noted was 5.32 MPa and 6.79 MPa at 28 and 90 days, respectively. Luukkonen et al. [65] have reported that slag-based one-part geopolymers with solid sodium silicate had flexural strengths ranging from 7.5 to 8.2 MPa at 28 days. Similarly, Ma et al. [69] reported flexural strengths between 7 and 8 MPa at both 28 and 56 days for their high-strength OP-GPC mixes. For split-tensile strength, Yip et al. [70] and Ming et al. [67] observed values between 5 and 6.5 MPa for mixes with compressive strengths above 60 MPa.

The measured values of change in weight and compressive strength of high-strength OP-GPC after sulphate immersion are presented in Fig. 3. The dotted reference line presented in the figure represents the weight and compressive strength of cylindrical samples cured in water for 28 days and termed as controlled specimens. The weight change and strength in compression at various exposure period was determined with respect to controlled specimen.

The weight of controlled specimen was 3.84 Kg which increased to 3.87 kg, 3.90 kg and 3.84 kg after the exposure of specimens in the sulphate solution for 28, 56 and 90 days, respectively. The weight of samples was noted to decrease up to 3.81 kg and 3.80 kg when subjected to sulphate-rich environments for 120 and 180 days, respectively. Results showed a marginal increase of 0.8 % in weight of specimens up to 90 days of exposure period in sulphate solution and thereafter a decrease in weight of 1.0% for the exposure period of 180 days. The initial increase in weight up to 90 days is attributed to the formation of ettringite and gypsum in voids and decrease in weight at later ages is attributed to migration of alkalis from solid specimen to solution [71-72]. The compressive strength of controlled specimen was 70.46 MPa which increased to 74.00 MPa,

(a) (b)

Figure 4. Physical appearance of the specimens high-strength one- part GPC exposed to (a) sulphate solution (b) chloride solution for 180 days

77 MPa and 74.31 MPa after the exposure of specimens in the sulphate solution for 28, 56 and 90 days, respectively, Fig. 3(b). The compressive strength of specimens was noted to decrease to 69.00 MPa and 68.12 MPa when exposed to sulphate solution for 120 days and 180 days, respectively. Results showed a marginal increase of 5.5% in strength of specimens up to 90 days of exposure period in sulphate solution and thereafter decrease of 3.3% for the exposure period of 180 days. The increase in strength up to 90 days is attributed to the continued polymerization and interlocking of the geopolymeric binder that enhances the bonding between particles and the development of a dense, 3D network that significantly improves the strength. However, further decrease in strength of the concrete could be attributed to the ongoing degradation process that causes crack formation and dissolution in microstructural and geopolymer bonds in the solvent [72]. The physical appearance of a typical specimen exposed to sulphate solution for 180 days is presented in Fig. 4(a), which showed that concrete is stable, sound and in shape with firm edges. Contrary to this, the conventional concrete exposed to 5% concentrated solution of magnesium sulphate for 180 days was reported in deteriorated state 120-140 days [73-74].

The chloride resistance of high-strength OP- GPC was measured in terms of change in weight and depth of chloride penetration at different exposure periods in a chloride solution. The measured weights of the cylindrical specimens were 3.89 Kg, 3.88 Kg, 3.88 Kg, 3.85 Kg and 3.80 Kg for the control specimens and at the exposure period of 56, 90, 120 and 180 days, respectively. The change in weight of the cylindrical specimens was not significant when exposed to the chloride solution even up to 180 days. Similar observations in respect to change in weight of OP- GPC exposed to chloride solution was reported by [75-78]. The measured values of the depth of chloride penetration of high-strength OP- GPC are presented in Fig. 5. The figure shows that depth of chloride penetration increased with increase in exposure period for of concrete. The penetration depth for high-strength OP- GPC was 1.10 mm, 1.70 mm and 2.01 mm and 5.81 mm when exposed to 56, 90, 120 and 180 days, respectively. The chloride diffusion coefficient (C_d) was also determined for all the specimens in accordance to ASTM C1556 [50]. The C_d measured for high-

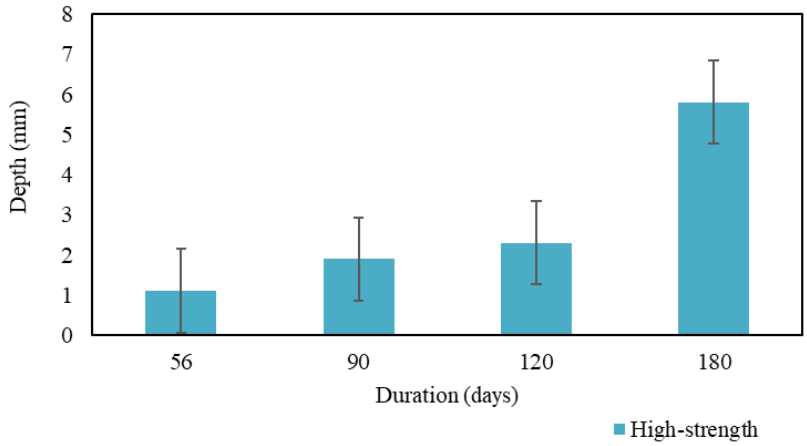

Figure 5. Measured values of chloride penetration depth for high -strength OP- GPC

Table 5. Measured values of density, absorption and voids of high-strength OP-GPC

Measured properties	High-strength OP- GPC
Absorption after immersion, (%)	3.40
Absorption after immersion and boiling, %	3.13
Bulk density, dry (g/m^3)	2.61
Bulk density after immersion (g/m^3)	2.70
Bulk density after immersion and boiling, %	2.69
Apparent density (g/m^3)	2.84
Volume of permeable pore space (voids), %	8.17

strength OP- GPC was 2.74 x 10^{-13} m²/s, 4.08 x 10^{-13} m²/s, 4.28 x 10^{-13} m²/s, 2.38 x 10^{-12} m²/s after exposure periods of 56 days, 90 days, 120 days and 180 days, respectively, in chloride solution. Results determined in terms of diffusion coefficient showed better resistance to chloride penetration in high-strength OP- GPC and also in good agreement with the results measured in terms of chloride penetration depth. The chloride penetration depth obtained for high- strength OP-GPC was 5.86 mm after a maximum duration of 180 days, however conventional concrete typically shows a greater chloride penetration depth, often exceeding 20 mm to 30 mm under similar conditions, due to its higher porosity and permeability [79-81].

The density, water absorption, and volume of permeable voids measured for high-strength OP-geopolymer concrete (GPC) in accordance with ASTM C642 [51] are presented in the Table 5.

The absorption rate after immersion was noted as 3.40%, while the absorption rate after immersion and boiling slightly decreased to 3.13%, indicating enhanced durability properties. The bulk density values further confirm the material's compactness, with a dry bulk density of 2.61 g/m³, which increased to 2.70 g/m³ after immersion and slightly reduced to 2.69 g/m³ after immersion and boiling. The apparent density was measured at 2.84 g/m³, showcasing the dense microstructure of high-strength GPC. Additionally, the volume of permeable voids was found to be 8.17%, which is lower than that of normal- and medium-strength GPC reported in previous studies.

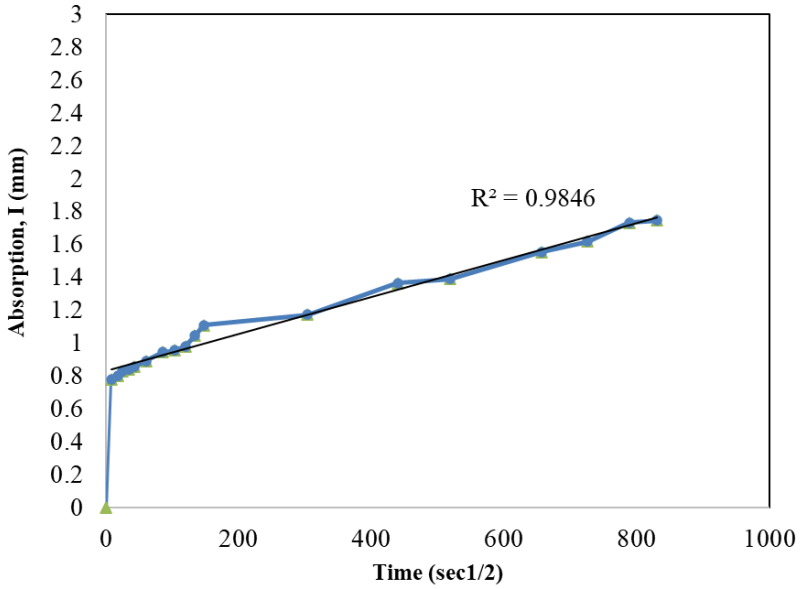

Fig. 6 Measured values of absorption of high- strength OP-GPC

The results revealed that high-strength OP-GPC made with GGBS and anhydrous metasilicate exhibits denser microstructure and reduced permeable voids compared to conventional geopolymer concrete and cement-based concrete reported in literature [82-85].

The absorption (I) values of high-strength OP- GPC plotted against the square root of time ($S^{1/2}$) are presented in Fig. 6. The I-values of the concrete samples was computed by dividing the change in mass with the product of cross-sectional area of the test specimen and density of water following ASTM C1585 [52]. In high-strength OP- GPC, the absorption values increased from 0.7771 mm to 1.1083 mm in a period from 60 seconds to 6 hours, corresponding to primary absorption. Further, the I- values increased from 1.3631 mm to 1.7452 mm in a period from 1 day to 7 days corresponding to secondary absorption. Results showed that high-strength OP- GPC exhibited low absorption values relative to normal-and medium-strength OP- GPC. The initial rate of absorption (sorptivity) of water was determined as the slope of the best-fit line plotted between I and $S^{1/2}$ and was found to be equal to 0.0022 mm/$s^{1/2}$ high-strength OP- GPC. The secondary sorptivity was noted as 0.0010 mm/$s^{1/2}$ high-strength OP- GPC. The low absorption values and sorptivity in the case of high-strength OP- GPC is attributed to its dense microstructure and the number of less permeable voids.

The depth of water penetration for high- strength OP- GPC was measured in accordance to IS 516 Part 2-sec 1 [53]. on the cube specimens subject to under pressure. The depth of water penetration measured in high-strength OP- GPC was 9.5 mm. The low depth of water penetration in case of high-strength OP- GPC is attributed to dense microstructure and less volume of permeable voids relative to normal-strength concrete.

The high-strength one-part GPC exhibited initial surface absorption values of 0.217 ml/m²/sec, 0.121 ml/m²/sec and 0.101 ml/m²/sec, at an interval of 10 minutes, 30 minutes, and 60 minutes, respectively. Results showed that the absorption values decreased over time in one-part GPC. The behavior is attributed to the fact that pores fills with the water over time and contribute to

impermeable. The absorption values in case of high-strength one-part GPC were significantly low that predicted reduced permeability of the high-strength one-part GPC.

5. Conclusions

The key conclusions from the experimental work are as follows:

• The mix design of high-strength OP- GPC was obtained through response surface methodology and was experimentally validated, encouraging its use in formulating and assessing concrete mix designs in construction practices.

• The compressive strength obtained for high-strength OP-GPC was 66.14 MPa at 7 days and 71.25 MPa at 28 days. Notably, over 90% of the 28-day strength was achieved within 7 days, indicating rapid early-age strength gain. For high-strength OP-GPC, the flexural strength of the concrete mixes reported was measured at 7.37 MPa after 28 days that increased to 8.08 MPa at 90 days. The split-tensile strength noted was 5.32 MPa and 6.79 MPa at 28 and 90 days, respectively.

• Upon exposure to 5% magnesium sulfate solution, high-strength OP- GPC specimens initially showed a marginal weight increase of 0.8% up to 90 days due to ettringite and gypsum formation, followed by a 1% weight loss at 180 days, attributed to alkali migration. The compressive strength increased by 5.5% up to 90 days. The increase in strength up to 90 days is attributed to the continued polymerization and interlocking of the geopolymeric binder that enhances the bonding between particles and the development of a dense, 3D network that significantly improves the strength. Further a decrease in the strength upto 3.3% was noted after 180 days, due to degradation. Physical inspection after 180 days showed the specimens remained stable and intact, unlike conventional concrete, which typically exhibits surface deterioration under similar conditions.

• The depth of chloride penetration increased with the exposure period, measuring 1.10 mm at 56 days, 1.70 mm at 90 days, 2.01 mm at 120 days, and 5.81 mm at 180 days in 5% sodium chloride solution. The measured chloride diffusion coefficient (Cd) also increased over time, but remained lower than conventional concrete, confirming better resistance. Notably, the maximum depth of penetration (5.81 mm at 180 days) is substantially lower than values reported for ordinary cement concrete (typically >20 mm under similar conditions).

• The high-strength OP- GPC exhibited a dry bulk density of 2.61 g/cm^3, increasing to 2.70 g/cm^3 after immersion, and 2.69 g/cm^3 after immersion and boiling. The apparent density was measured as 2.84 g/cm^3. Water absorption was 3.40% after immersion and 3.13% after immersion and boiling. The volume of permeable voids was 8.17%, notably low value that indicated a denser and less porous matrix.

• The initial and secondary sorptivity values for high-strength OP- GPC were 0.0022 mm/S$^{1/2}$ and 0.0010 mm/S$^{1/2}$, respectively, demonstrating reduced water uptake relative to lower strength grades. The depth of water penetration was measured as 9.5 mm, which is lower than conventional concrete, further confirming the dense microstructure and reduced permeability of the high-strength mix.

• The depth of water penetration measured in high-strength OP- GPC was 9.5 mm. The high-strength one-part GPC exhibited initial surface absorption values of 0.217 ml/m^2/sec, 0.121 ml/m^2/sec and 0.101 ml/m^2/sec, at an interval of 10 minutes, 30 minutes, and 60 minutes, respectively.

Acknowledgement

The authors acknowledge the resources of Concrete Technology Laboratory, Department of Civil Engineering, Central University of Haryana for their support in conducting the experiments reported in this research paper.

References

1. BIS 456 (2021). Plain and reinforced concrete – Code of practice. Bureau of Indian Standards, New Delhi, India.
2. Neupane, K. (2018). High-strength geopolymer concrete: Properties, advantages and challenges. Advances in Materials, 7(2), 15. https://doi.org/10.11648/j.am.20180702.11.
3. Sujitha, V.S., Raja, S., Rusho, M.A., Yishak, S. (2025). Advances and developments in high-strength geopolymer concrete for sustainable construction – A review. Case Studies in Construction Materials, 22, e04669. https://doi.org/10.1016/j.cscm.2025.e04669.
4. Weil, M., Dombrowski, K., Buchwald, A. (2009). Life-cycle analysis of geopolymers. Geopolymers: Structure, Processing, Properties and Industrial Applications. Elsevier, Oxford, UK. https://doi.org/10.1533/9781845696382.2.194.
5. Fang, Y., Wang, C., Yang, H., Chen, J., Dong, Z., Li, L. (2024). Development of a ternary high-temperature resistant geopolymer and the deterioration mechanism of its concrete after heat exposure. Construction and Building Materials, 449, 138291. https://doi.org/10.1016/j.conbuildmat.2024.138291.
6. Kanagaraj, B., Lubloy, E., Anand, N., Hlavicka, V., Kiran, T. (2023). Investigation of physical, chemical, mechanical, and microstructural properties of cement-less concrete – State-of-the-art review. Construction and Building Materials, 365, 130020. https://doi.org/10.1016/j.conbuildmat.2022.130020.
7. Moradikhou, A.B., Safehian, M., Golafshani, E.M. (2023). High-strength geopolymer concrete based on coal washing waste. Construction and Building Materials, 362, 129675. https://doi.org/10.1016/j.conbuildmat.2022.129675.
8. Nodehi, M., Ozbakkaloglu, T., Gholampour, A., Mohammed, T., Shi, X. (2022). The effect of curing regimes on physico-mechanical, microstructural and durability properties of alkali-activated materials: A review. Construction and Building Materials, 321, 126335. https://doi.org/10.1016/j.conbuildmat.2022.126335.
9. Zeyad, A.M., Bayagoob, K.H., Amin, M., Tayeh, B.A., Mostafa, S.A., Agwa, I.S. (2024). Effect of olive waste ash on the properties of high-strength geopolymer concrete. Structural Concrete, 26(2), 1206-1225. https://doi.org/10.1002/suco.202400035.
10. Hajimohammadi, A., Provis, J.L., van Deventer, J.S.J. (2008). One-part geopolymer mixes from geothermal silica and sodium aluminate. Industrial and Engineering Chemistry Research, 47(23), 9396-9405. https://doi.org/10.1021/ie8005825.
11. Jindal, B.B. (2018). Feasibility study of ambient cured geopolymer concrete - A review. Advances in Concrete Construction, 6(4), 387-405. https://doi.org/10.12989/acc.2018.6.4.387.
12. Mahendra, K., Narasimhan, M.C., Bhanu Prakash, G., Das, A.K. (2024). Multi-objective optimization of one-part alkali-activated mortar mixes using Taguchi-Grey relational analysis. Construction and Building Materials, 412, 134761. https://doi.org/10.1016/j.conbuildmat.2023.134761.
13. Panitsa, O.A., Kioupis, D., Kakali, G. (2023). Application of silica fume-based solid activators for the one-part geopolymerization of aluminosilicate raw materials. Materials Today: Proceedings, (in press) Advance online publication. https://doi.org/10.1016/j.matpr.2023.07.204.
14. Sharma, D., Singh, R.B. (2025). Durability characteristics of normal- and medium-strength one-part geopolymer concrete. Advances in Concrete Construction, 20(3), 167-185. https://doi.org/10.12989/acc.2025.20.3.167.
15. Sharma, D., Singh, R.B., Gupta, A. (2025). A state-of-the-art review on development and properties of

one-part geopolymer materials. Advances in Civil Engineering, 2025, Article 8856426, 1-28. https://doi.org/10.1155/adce/8856426.
16. Chowdhury, S., Mohapatra, S., Gaur, A., Dwivedi, G., Soni, A. (2021). Study of various properties of geopolymer concrete - A review. Materials Today: Proceedings, 46, 5687-5695. https://doi.org/10.1016/j.matpr.2020.09.835.
17. Kathirvel, P., Sreekumaran, S. (2021). Sustainable development of ultra-high performance concrete using geopolymer technology. Journal of Building Engineering, 39, 102267. https://doi.org/10.1016/j.jobe.2021.102267.
18. Li, Y., Shen, J., Lin, H., Li, Y. (2023). Optimization design for alkali-activated slag-fly ash geopolymer concrete based on artificial intelligence considering compressive strength, cost and carbon emission. Journal of Building Engineering, 75, 106929. https://doi.org/10.1016/j.jobe.2023.106929.
19. Swathi, B., Vidjeapriya, R. (2023). Influence of precursor materials and molar ratios on normal, high and ultra-high performance geopolymer concrete - A state-of-the-art review. Construction and Building Materials, 392, 132006. https://doi.org/10.1016/j.conbuildmat.2023.132006.
20. Dong, M., Elchalakani, M., Karrech, A. (2020). Development of high-strength one-part geopolymer mortar using sodium metasilicate. Construction and Building Materials, 236, 117611. https://doi.org/10.1016/j.conbuildmat.2019.117611.
21. Dakhane, A., Neithalath, N. (2022). Reaction kinetics and characterization of slag-based high-strength just-add-water one-part alkali-activated binders. Recent Progress in Materials, 4(2), 6. https://doi.org/10.21926/rpm.2202006.
22. Manjunath, H., Cheng-Yong, H., Yun-Ming, L. (2023). Strength optimization and key factor correlation of one-part fly ash/ladle furnace slag (FA/LFS) geopolymer using statistical approach. Journal of Building Engineering, 63, 105480. https://doi.org/10.1016/j.jobe.2022.105480.
23. Araújo Júnior, N.T., Lima, M.E.V., Torres, S.M., Basto, P.E.A., Melo Neto, A.A. (2021). Experimental investigation of mix design for high-strength alkali-activated slag concrete. Construction and Building Materials, 291, 123387. https://doi.org/10.1016/j.conbuildmat.2021.123387.
24. Sharma, D., Singh, R.B. (2024). Strength-based design mix methodology of one-part geopolymer concrete using response surface methodology. Multiscale and Multidisciplinary Modeling, Experiments and Design, 8(1). https://doi.org/10.1007/s41939-024-00713-y.
25. Kurtoglu, A.E., Kaya, M., Eren, N.A. (2025). Modeling the strength of geopolymer concrete at high temperatures: Machine learning approach. Computers and Concrete, 35(6), 669-685. https://doi.org/10.12989/cac.2025.35.6.669.
26. Paruthi, S., Rahman, I., Husain, A. (2023). Comparative studies of different machine learning algorithms in predicting the compressive strength of geopolymer concrete. Computers and Concrete, 32(6), 607-613. https://doi.org/10.12989/cac.2023.32.6.607.
27. Al-Rousan, R.Z., Sawalha, H.M. (2024). The behavior of concrete filled steel tubular columns infilled with high-strength geopolymer recycled aggregate concrete. Steel and Composite Structures, 51(6), 661-678. https://doi.org/10.12989/scs.2024.51.6.661.
28. Khater, H.M., Abd el Gawaad, H.A. (2015). Characterization of alkali activated geopolymer mortar doped with MWCNT. Advances in Materials Research, 4(1), 45-61. https://doi.org/10.12989/amr.2015.4.1.45.
29. Driouich, A., El Alami El Hassani, S., Zmirli, Z., El Harfaoui, S., Sor, N.H., Aziz, A., Hu, J.W., Isleem, H.F., Najm, H.M., Chaair, H. (2024). Investigation of physicochemical properties, sustainability and environmental evaluation of metakaolin-granulated blast furnace slag geopolymer concrete. Computers and Concrete, 34(4), 489-501. https://doi.org/10.12989/cac.2024.34.4.489.
30. Zedan, S.R., Mohamed, M.R., Ahmed, D.A., Mohammed, A.H. (2015). Alkali activated ceramic waste with or without two different calcium sources. Advances in Materials Research, 4(3), 133-144. https://doi.org/10.12989/amr.2015.4.3.133.
31. Martinez-Conesa, E.J., Egea, J.A., Miguel, V., Toledo, C., Meseguer-Valdenebro, J.L. (2017). Optimization of geometric parameters in a welded joint through response surface methodology. Construction and Building Materials, 154, 105-114. https://doi.org/10.1016/j.conbuildmat.2017.07.163.

32. Breig, S.J.M., Luti, K.J.K. (2021). Response surface methodology: A review on its applications and challenges in microbial cultures. Materials Today: Proceedings, 42, 2277-2284. https://doi.org/10.1016/j.matpr.2020.12.316.
33. Bianco, I., Ap Dafydd Tomos, B., Vinai, R. (2021). Analysis of the environmental impacts of alkali-activated concrete produced with waste glass-derived silicate activator - A LCA study. Journal of Cleaner Production, 289, 128383. https://doi.org/10.1016/j.jclepro.2021.128383.
34. Elzeadani, M., Bompa, D.V., Elghazouli, A.Y. (2022). Experimental assessment and constitutive modelling of rubberised one-part alkali-activated concrete. Construction and Building Materials, 344, 129161. https://doi.org/10.1016/j.conbuildmat.2022.129161.
35. Haruna, S., Mohammed, B.S., Wahab, M.M.A., Liew, M.S. (2020). Effect of paste-aggregate ratio and curing methods on the performance of one-part alkali-activated concrete. Construction and Building Materials, 243, 120024. https://doi.org/10.1016/j.conbuildmat.2020.120024.
36. Li, N., Shi, C., Zhang, Z., Zhu, D., Hwang, H.J., Zhu, Y., Sun, T. (2018). A mixture proportioning method for the development of performance-based alkali-activated slag-based concrete. Cement and Concrete Composites, 93, 163-174. https://doi.org/10.1016/j.cemconcomp.2018.07.009.
37. Liu, Q., Cai, Y., Peng, H., Meng, Z., Mundra, S., Castel, A. (2023). A numerical study on chloride transport in alkali-activated fly ash/slag concretes. Cement and Concrete Research, 166, 107094. https://doi.org/10.1016/j.cemconres.2023.107094.
38. Mavroulidou, M., Sanam, I., Mengasini, L. (2023). Mechanical and durability performance of alkali-activated slag cement concretes with carbonate and silicate activators. Sustainable Chemistry and Pharmacy, 34, 100896. https://doi.org/10.1016/j.scp.2022.100896.
39. Neupane, K., Hadigheh, S.A. (2021). Sodium hydroxide-free geopolymer binder for prestressed concrete applications. Construction and Building Materials, 270, 123397. https://doi.org/10.1016/j.conbuildmat.2021.123397.
40. Okoro, W., Oyebisi, S. (2023). Mechanical and durability assessments of steel slag-seashell powder-based geopolymer concrete. Heliyon, 9(2), e13188. https://doi.org/10.1016/j.heliyon.2023.e13188.
41. BIS 16714 (2018). Product manual for ground granulated blast furnace slag for use in cement, mortar and concrete. Bureau of Indian Standards, New Delhi, India.
42. BIS 383 (2016). Specification for coarse and fine aggregates from natural sources for concrete. Bureau of Indian Standards, New Delhi, India.
43. BIS 2386 (2021). Methods of test for aggregates for concrete, Part 4: Mechanical properties. Bureau of Indian Standards, New Delhi, India.
44. BIS 4031 (2021). Methods of physical tests for hydraulic cement. Bureau of Indian Standards, New Delhi, India.
45. BIS 1199 (2018). Methods of sampling and analysis of concrete. Bureau of Indian Standards, New Delhi, India.
46. BIS 516 (2021). Method of tests for strength of concrete: Compressive strength of concrete. Bureau of Indian Standards, New Delhi, India.
47. Alabi, S.A., Mahachi, J. (2021). Chloride ion penetration performance of recycled concrete with different geopolymers. Materials Today: Proceedings, 38, 762-766. https://doi.org/10.1016/j.matpr.2020.04.199.
48. BIS 5816 (2018). Method of test for splitting tensile strength of concrete. Bureau of Indian Standards, New Delhi, India.
49. GB/T 50082 (2024). Standard for test methods of long-term performance and durability of concrete. China Architecture & Building Press, Beijing, China.
50. ASTM C1556 (2022). Standard test method for determining the apparent chloride diffusion coefficient of cementitious mixtures by bulk diffusion. ASTM International, West Conshohocken, PA, USA.
51. ASTM C642 (2021). Standard test method for density, absorption, and voids in hardened concrete. ASTM International, West Conshohocken, PA, USA.
52. ASTM C1585 (2020). Standard test method for measurement of rate of absorption of water by hydraulic-cement concretes. ASTM International, West Conshohocken, PA, USA.

53. BIS 516 (Part 2/Sec 1) (2021). Hardened concrete - Methods of test, Part 2: Properties of hardened concrete other than strength, Section 1: Density and depth of water penetration. Bureau of Indian Standards, New Delhi, India.
54. BS 1881: Part 208 (1996). Recommendations for the determination of the initial surface absorption of concrete. British Standards Institution, London, UK.
55. BS EN 12390-2 (2019). Testing hardened concrete - Part 2: Making and curing specimens for strength tests. British Standards Institution, London, UK.
56. Janga, S., Raut, A.N., Adamu, M., Ibrahim, Y.E., Albuaymi, M. (2024). Multi-response optimization of thermally efficient RC-based geopolymer binder using response surface methodology approach. Developments in the Built Environment, 19, 100528. https://doi.org/10.1016/j.dibe.2024.100528.
57. Shi, X., Zhang, C., Wang, X., Zhang, T., Wang, Q. (2022). Response surface methodology for multi-objective optimization of fly ash-GGBS-based geopolymer mortar. Construction and Building Materials, 315, 125644. https://doi.org/10.1016/j.conbuildmat.2021.125644.
58. Zahid, M., Shafiq, N., Isa, M.H., Gil, L. (2018). Statistical modeling and mix design optimization of fly ash-based engineered geopolymer composite using response surface methodology. Journal of Cleaner Production, 194, 483-498. https://doi.org/10.1016/j.jclepro.2018.05.158.
59. Draper, N.R., Smith, H. (1998). Applied regression analysis (3rd ed.). Wiley, Hoboken, NJ, USA. https://doi.org/10.1002/9781118625590.
60. Teo, W., Shirai, K., Lim, J.H., Jack, L.B., Nikbakht, E. (2022). Experimental investigation on ambient-cured one-part alkali-activated binders using combined high-calcium fly ash and ground granulated blast furnace slag. Materials, 15(4), 1612. https://doi.org/10.3390/ma15041612.
61. Ganesan, K., Rajagopal, K., Thangavel, K. (2008). Rice husk ash blended cement: Assessment of optimal level of replacement for strength and permeability properties of concrete. Construction and Building Materials, 22(8), 1675-1683. https://doi.org/10.1016/j.conbuildmat.2007.06.011.
62. Jiang, C., Fan, K., Wu, F., Chen, D. (2014). Experimental study on the mechanical properties and microstructure of chopped basalt fibre reinforced concrete. Materials & Design, 58, 187-193. https://doi.org/10.1016/j.matdes.2014.01.056.
63. Poon, C.S., Shui, Z.H., Lam, L., Fok, H., Kou, S.C. (2004). Influence of moisture states of natural and recycled aggregates on the slump and compressive strength of concrete. Cement and Concrete Research, 34(1), 31-36. https://doi.org/10.1016/S0008-8846(03)00186-8.
64. Rahal, K. (2007). Mechanical properties of concrete with recycled coarse aggregate. Building and Environment, 42(1), 407-415. https://doi.org/10.1016/j.buildenv.2005.07.033.
65. Luukkonen, T., Abdollahnejad, Z., Yliniemi, J., Kinnunen, P., Illikainen, M. (2018). One-part alkali-activated materials: A review. Cement and Concrete Research, 103, 21-34. https://doi.org/10.1016/j.cemconres.2017.10.001.
66. Ma, C., Zhao, B., Guo, S., Long, G., Xie, Y. (2019). Properties and characterization of green one-part geopolymer activated by composite activators. Journal of Cleaner Production, 220, 188-199. https://doi.org/10.1016/j.jclepro.2019.02.159.
67. Ming, L.Y., En, O.W., Yong, H.C., Abdullah, M.M.A.B., Ween, O.S. (2021). Characteristic of one-part geopolymer as building materials. Lecture Notes in Civil Engineering, 129, 97-118. Springer, Singapore. https://doi.org/10.1007/978-981-33-4918-6_6.
68. Wang, Y.S., Alrefaei, Y., Dai, J.G. (2021). Roles of hybrid activators in improving the early-age properties of one-part geopolymer pastes. Construction and Building Materials, 306, 124880. https://doi.org/10.1016/j.conbuildmat.2021.124880.
69. Ma, Y., Hu, J., Ye, G., van Breugel, K. (2023). Assessing the viability of a high-performance one-part geopolymer made from fly ash and GGBS at ambient temperature. Journal of Building Engineering, 65, 105616. https://doi.org/10.1016/j.jobe.2022.105616.
70. Yip, C.K., Lukey, G.C., van Deventer, J.S.J. (2007). The coexistence of geopolymeric gel and calcium silicate hydrate at the early stage of alkaline activation. Cement and Concrete Research, 37(12), 1531-1539. https://doi.org/10.1016/j.cemconres.2007.08.014.
71. Albitar, M., Mohamed Ali, M.S., Visintin, P., Drechsler, M. (2017). Durability evaluation of

geopolymer and conventional concretes. Construction and Building Materials, 136, 374-385. https://doi.org/10.1016/j.conbuildmat.2017.01.056.
72. Elyamany, H.E., Abd Elmoaty, A.E.M., Elshaboury, A.M. (2018). Magnesium sulfate resistance of geopolymer mortar. Construction and Building Materials, 184, 111-127. https://doi.org/10.1016/j.conbuildmat.2018.06.212.
73. Bakharev, T. (2005). Durability of geopolymer materials in sodium and magnesium sulfate solutions. Cement and Concrete Research, 35(6), 1233-1246. https://doi.org/10.1016/j.cemconres.2004.09.002.
74. Mostofinejad, D., Nosouhian, F., Nazari-Monfared, H. (2016). Influence of magnesium sulphate concentration on durability of concrete containing micro-silica, slag and limestone powder using durability index. Construction and Building Materials, 117, 107-120. https://doi.org/10.1016/j.conbuildmat.2016.04.091.
75. Chen, K., Wu, D., Xia, L., Cai, Q., Zhang, Z. (2021). Geopolymer concrete durability subjected to aggressive environments - A review of influence factors and comparison with ordinary Portland cement. Construction and Building Materials, 279, 122496. https://doi.org/10.1016/j.conbuildmat.2021.122496.
76. Jia, R., Wang, Q., Luo, T. (2023). Mechanisms and differences between sodium and magnesium sulfate attacks on alkali-activated phosphorus slag. Construction and Building Materials, 403, 133117. https://doi.org/10.1016/j.conbuildmat.2023.133117.
77. Wang, X., Lan, Q., Lin, H., Wang, Y., Wu, W., Xu, L., Fu, L., Li, C. (2024). Effects of alkali activator on the chloride-ion permeability of one-part alkali-activated nickel slag concrete. Case Studies in Construction Materials, 20, e02970. https://doi.org/10.1016/j.cscm.2024.e02970.
78. Xu, Z., Ye, G. (2023). Understanding chloride diffusion coefficient in cementitious materials. Materials, 16(9), 3464. https://doi.org/10.3390/ma16093464.
79. Althoey, F. (2021). Compressive strength reduction of cement pastes exposed to sodium chloride solutions: Secondary ettringite formation. Construction and Building Materials, 299, 123965. https://doi.org/10.1016/j.conbuildmat.2021.123965.
80. Costa, A., Appleton, J. (1999). Chloride penetration into concrete in marine environment - Part I: Main parameters affecting chloride penetration. Materials and Structures, 32(4), 252-259. https://doi.org/10.1007/BF02479594.
81. Du, F., Jin, Z., She, W., Xiong, C., Feng, G., Fan, J. (2020). Chloride ions migration and induced reinforcement corrosion in concrete with cracks: A comparative study of current acceleration and natural marine exposure. Construction and Building Materials, 263, 120099. https://doi.org/10.1016/j.conbuildmat.2020.120099.
82. Assi, L.N., Deaver, E.E., Ziehl, P. (2018). Effect of source and particle size distribution on the mechanical and microstructural properties of fly ash-based geopolymer concrete. Construction and Building Materials, 167, 372-380. https://doi.org/10.1016/j.conbuildmat.2018.01.193.
83. Kristiawan, S.A., Sunarmasto, Murti, G.Y. (2017). Porosity of self-compacting concrete (SCC) incorporating high volume fly ash. Proceedings of the International Conference on Advanced Materials for Better Future, Surakarta, Indonesia, October. https://doi.org/10.1088/1757-899X/176/1/012043.
84. Şahmaran, M., Li, V.C. (2009). Influence of microcracking on water absorption and sorptivity of ECC. Materials and Structures, 42(5), 593-603. https://doi.org/10.1617/s11527-008-9406-6.
85. Tay, C.H., Mazlan, N., Wayayok, A., Basri, M.S., Mustafa, M., Abdullah, A. (2022). Nanocellulose reinforced zeolite-based geopolymer concrete: Density analysis through response surface methodology. Materials Today: Proceedings, 66, 2873-2882. https://doi.org/10.1016/j.matpr.2022.06.550.